The final publication is available at

http://dx.doi.org/10.1016/j.energy.2015.03.130

Additional Information

Turbocharger heat transfer and mechanical losses influence in predicting engines performance by using one-dimensional simulation codes

José Ramón Serrano, Pablo Olmeda*, Francisco J. Arnau, Artem Dombrovsky

CMT-Motores Térmicos, Universitat Politècnica de València, Camino de Vera s/n. 46022 València, Spain

Les Smith

Jaguar Cars Limited, JLR Powertrain Analysis, Abbey Road, Whitley, Coventry, CV3 4LF, UK

Abstract

The exhaust energy can represent up to 40% of the fuel chemical energy in turbocharged internal combustion engines. In order to calculate properly the available energy of the exhaust gases, a critical parameter is the temperature downstream the turbine. The prediction of this temperature will also benefit the two-stage turbochargers and after-treatment modelling that affects brake specific fuel consumption, exhaust gases emissions and the scavenging process.

In this paper, turbocharger heat transfer losses have been modelled using a lumped capacitance model coupled with one-dimensional whole-engine simulation software. The data from the simulations of a turbocharged Diesel engine, with and without the turbocharger heat transfer model, have been compared with experimental measurements performed in an engine test bench. The analysis is focused on studying the influence in turbocharger outlet temperatures and predicting the engine performance. The main result of the study is the improvement in the prediction of both compressor and turbine outlet temperatures (up to an improvement of 70 K). The results from the model allow analysing how

---

*Corresponding author
Email address: `pabolgon@mot.upv.es` (Pablo Olmeda)
URL: `www.cmt.upv.es` (Pablo Olmeda)

heat transfer losses are split in the turbocharger and quantifying the importance of heat transfer phenomena in turbocharger efficiency, at full load conditions and as a function of engine speed.

Nomenclature

a	Sensor uncertainty	$-$
c_p	Specific heat capacity	$\mathrm{J \cdot kg^{-1} \cdot K^{-1}}$
h	Specific enthalpy	$\mathrm{J \cdot kg^{-1}}$
K	Turbocharger speed constant	rpm/W
p	Pressure	Pa
s	Specific entropy	$\mathrm{J \cdot kg^{-1} \cdot K^{-1}}$
n	Number of measurements	$-$
N	Turbocharger speed	rpm
T	Temperature	K
$\dot{m}$	Mass flow	$\mathrm{kg \cdot s^{-1}}$
$\dot{Q}$	Heat flow	W
u	Standard deviation	$-$
$\dot{W}$	Mechanical power	W
$\dot{W}'$	Mechanical and heat power	W

Greek symbols

η	Efficiency	$-$
Δ	Increment or drop	$-$

Subscripts and superscripts

0	Total conditions
1	Compressor inlet
2	Compressor outlet
3	Turbine inlet
4	Turbine outlet
a, $adiab.$	Adiabatic conditions
c	Refers to compressor
C	Compressor node
$diab.$	Diabatic conditions
GAS	Gas node
t	Refers to turbine

T	Turbine node
$H1$	Turbine housing node
$H2$	Central housing node
$H3$	Compressor housing node
W	Water node
IC	Compressor inlet
OC	Compressor outlet
OC_s	Isentropic compressor outlet
IT_1	Adiabatic turbine inlet
OT	Turbine outlet
OT_s	Isentropic turbine outlet
s	Isentropic
TG	Refers to turbocharger
$mech$	Refers to mechanical losses

Abbreviations

AC	Alternating current
BSFC	Brake specific fuel consumption
CALMEC$^{\text{TM}}$	Combustion diagnosis tool
CFD	Computational fluid dynamics
COT	Compressor outlet temperature
ECU	Engine control unit
EGR	Exhaust gas recirculation
ETE	Effective turbine efficiency
EVO	Exhaust valve opening
HT&ML	Heat transfer and mechanical losses model
ORC	Organic Rankine Cycle
TOT	Turbine outlet temperature
VGT	Variable geometry turbine

1. Introduction

The research on internal combustion engines is currently focused on energy optimisation and the reduction of fuel consumption and pollutant emissions. Different strategies to fulfil these objectives have been studied. Engine downsizing combined with a high level of turbocharging is one of these strategies [1]. Moreover, turbocharging affects other engine systems such as EGR [2], cooling and combustion; all of them related both with engine BSFC and engine emissions. In addition, the phenomena taking place internally to the turbocharger affect engine performance [3]. Turbocharger heat transfer is one of these phenomena. In order to estimate the heat fluxes in a turbocharger, working coupled to the engine, several approximations proposed by different authors can be employed, as described below.

Some authors have studied the phenomena experimentally, both in a gas stand [4] and in an engine test bench [5], while other studies are theoretical [6]. The gas stand tests aim to decouple the turbocharger phenomena from the ones associated to the engine. The engine test bench experiments represent the closest approximation to real vehicle operation conditions. An important effort has been made by some authors [7] in analysing different heat transfer conditions in the turbocharger on engine operation. These studies conclude that the importance of heat transfer phenomena in the overall power exchange inside the turbocharger can be significant at low and medium turbocharger speeds.

Other authors [8] have performed CFD (Computational Fluid Dynamics) studies in order to better understand the phenomena and their implications. These studies show the relevant heat transfer paths and their magnitude. However, due to computational limitations, this approach cannot be used if a whole engine has to be modelled.

The experimental approach is closer to the real application but it is inefficient in engine design because a test campaign of prohibitive economical cost would be needed. The CFD approach is able to save part of these costs but at high temporal costs and it cannot be used in a whole engine model (the

5

computational cost would be prohibitive). Between both options, a 1D modelling codes such as GT-Suite can be used, which are extensively used by engine manufacturers in design and research. This approach makes possible the prediction of variables related to both the engine and the turbocharger, crucial when overall conclusions are needed. Some authors have used this methodology in predicting different variables related to the engine and turbocharger system comparing with experimental results, and considering different approaches for the turbocharger [9].

The present work tries to clarify the strong debate about the influence of turbocharger heat transfer and mechanical losses (HT&ML, from now on) models on engine performance prediction. Some authors have performed experimental measurements in gas stand concluding that the effect of turbocharger heat transfer is irrelevant compared to turbocharger mechanical power at high engine loads [10]. However, more recent studies [11] show that heat transfer in the turbine always represent an important part of its enthalpy change, being more relevant in the low torque region. Some authors [12] have measured turbocharger performance in an engine test bench concluding that at high engine speeds and loads the deviation between adiabatic and non-adiabatic compressor efficiency is small. Nevertheless, other authors [13] have pointed that at higher powers the distribution of heat transfer during compression process has important effects. It is widely accepted that the influence of HT&ML models is important at part loads and at transient operation [14]. However, neither studies quantifying the influence of these models on engine parameters nor studies indicating the engine parameters affected are found in the literature. In the present work the importance of these models on full load simulations is shown.

In order to clarify this controversy, a simple lumped model able to predict heat transfer and mechanical losses phenomena in turbochargers is used, coupled with a complete engine model built in GT-Power. Engine full load conditions at different speeds have been simulated and compared with experimental results. Experimental tasks have been described in the first place; focusing on the description of test rig and equipment used; the different turbochargers and

6

engines that have been tested; the description of the testing methodology and the results of the tests. The second part of the paper is focused on the modelling work, starting with a brief description of the HT&ML model used, followed by a description of the engine model in GT-Power, and finishing with a description of the performed simulations. Then, a discussion of the obtained results with the different models and their comparison with experimental data is presented. Finally, the main conclusions of the work are summarised.

2. Experimental work

The experimental tasks of this work have been performed in an engine test bench using two different turbochargers (with and without water cooling) coupled to a 2 litres engine, but emulating 1.6 litres engine for the non water-cooled turbocharger (downspeeding).

2.1. Engine test bench

A schematic of the engine test bench is presented in Figure 1. It is a standard engine test rig, designed for the study of internal combustion engines up to 200 kW of power. The facility is assembled to control and evaluate the engine performance in steady and transient conditions. The most important devices of the engine test bench are:

- AC-Dynamometer, variable frequency and high response.

- High frequency analogical data acquisition system.

- Test room control device and data acquisition system.

- Continuous smoke measurement device.

- Control strategies design hardware.

- Air flow measurement system (hot-wire anemometer).
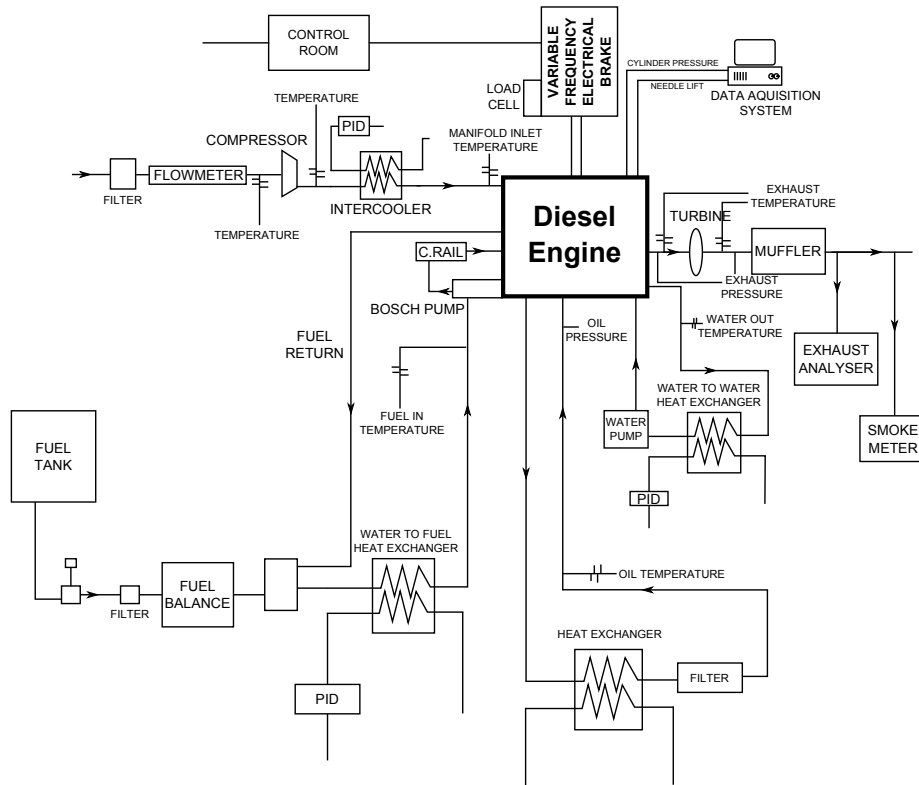
- Transient fuel-flow measurement balance.

7

Figure 1: Engine test bench layout

- Piezoelectric and piezoresistive cooled pressure transducer.

- Exhaust gas analyser.

- Thermocouples and Thermoresistances.

In an engine test bench the measurement conditions of the turbocharger offer less freedom than in a gas stand, although the test conditions are closer to the real operation of the turbocharger.

For the measurements of current work the uncertainty estimation was evaluated by using a statistical analysis from manufacturers data as it has been proposed in [15]. In Table 1 the uncertainty of the sensors is shown. The uncertainty due to the inaccuracy of each sensor is computed assuming uniform rectangular distribution of probability [16]. Equation 1 is used in this case.

8

Table 1: Characteristics of the main sensors

Variable	Sensor	Range / Uncertainty
Gas Pressure	Piezoresistive	$[0-5] \pm 0.025$ bar
Gas, and wall Temp.	K-type Therm.	$[-200 - +1200] \pm 2.2°$C
Gas Mass Flow	Hot wire	$[0-720] \pm 0.72$ kg/h
Oil Pressure	Piezoresistive	$[0-6] \pm 0.025$ bar
Oil Temperature	RTD	$[-200 - +650] \pm 0.15$ °C
Oil Flow	Coriolis	$[0-100]$ kg/h ± 0.1 %
Coolant Pressure	Piezoresistive	$[0-6] \pm 0.025$ bar
Coolant Temperature	RTD	$[-200 - +650] \pm 0.15$ °C
Coolant Flow	Magnetic	$[50-6000]$ kg/h ± 0.1 %
Fuel Mass	Fuel Balance	$[0-150]$ kg/h ± 0.12 %
Crankshaft Angle	Angular Encoder	$[1-20000]$ rpm $+0.02$ °

$$u_b = \sqrt{\frac{(a_+ - a_-)^2}{12}} \tag{1}$$

Finally, the measurement uncertainty is calculated using Equation 2, which yield a maximum uncertainty in enthalpy drops measurements of 2%.

$$u_c = \sqrt{\sum_{i=1}^{k} \left(\frac{\partial f}{\partial x_i}\right)^2 \cdot u^2\left(x_i\right)} \tag{2}$$

2.2. Turbochargers and engine characteristics

Two different turbochargers have been tested on engine. The main difference between them is the presence of water cooling and their characteristics are described in Table 2. A 2.0 litres HSDI engine is used for both turbochargers. Its main technical characteristics are presented in Table 3. Turbocharger T#1 is the original one of this engine, while for T#2 tests, downspeeding has been applied in order to avoid turbocharger overspeed. It means that engine speeds were adapted to emulate a 1.6 litre engine volumetric flow rate for the smaller

9

turbocharger (T#2). In this way full load engine points at different speeds have been measured for both turbochargers.

Table 2: Main characteristics of the employed turbochargers

Parameter	T#1	T#2
Turbine wheel diameter [mm]	41	38
Compressor wheel diameter [mm]	49	46
VGT	yes, vanes	yes, vanes
Water-cooling	yes	no
Matched to a characteristic engine displacement of [l]	2.0	1.6

Table 3: Main characteristics of the employed engine

Parameter	Value
Engine Displacement [cm^3]	1997
Bore [mm]	85
Stroke [mm]	88
Number of cylinders	4 in line
Valves	4 per cylinder
Compression ratio	16

110 *2.3. Engine full load tests*

Previously to the full load tests a set of different tests on the engine have been performed to characterise the valves flow coefficients and the combustion process in order to build an accurate 1D GT-Power engine model. Valves flow coefficients are important for calibrating the gas exchange process in the cylinder 115 and to predict intake mass flow correctly using the model. The characterisation of the combustion process is necessary for a good estimation of the in-cylinder conditions at the exhaust valve opening which affects the available energy at

10

the turbine inlet. This characterisation has been performed using instantaneous in-cylinder pressure signal from full load tests as will be described below.

120   Valves flow coefficients were obtained using a cold flow gas stand [17]. The cylinder head was disassembled from the engine and set up in a gas stand where the flow coefficients of intake and exhaust valves have been obtained for direct and reverse flow. The measurements were performed modifying the valve lift. These tests provided curves for all valves that correlated flow coefficients with

125   valve lift.

Combustion process was characterised using an in-house combustion diagnosis tool (CALMEC$^{\mathrm{TM}}$) [18], which is based on the measured instantaneous in-cylinder pressure and the characterization of some uncertainties [19]. From this measurement and other parameters that define the engine working point,

130   CALMEC$^{\mathrm{TM}}$is able to determine the heat release law by using the first principle of thermodynamics. The main objective of this task is to provide enough information to predict the in-cylinder conditions at the exhaust valve opening and then the fluid thermal state at turbine inlet.

Obtained experimental results from engine tests will be shown and they will

135   be further discussed when compared with modelling data.

3. Modelling work

The modelling work is divided in three parts. In the first part a HT&ML model has been developed on the basis of previous works done by the authors and programmed as user function in a commercial code for engine simulations

140   called GT-Power. Then, an engine model has been developed and validated in GT-Power environment. Finally, simulations with and without the HT&ML model have been performed in order to analyse the benefits and drawbacks of this model in engine simulations.

3.1. Turbocharger heat transfer and mechanical losses model

145   The main objective of the HT&ML model is the easiness to be used coupled with a general purpose models like GT-Power. For that reason, a 1D lumped

11

model is chosen as described in [20] and presented in Figure 2. In the model, the turbocharger has been divided in five metal nodes: one for the turbine case, one for the compressor case and three for the bearing housing. The variables of this model have been computed using experimental data provided by tests performed in specific test rigs, saving the costs of engine bench tests. On one hand, the thermal properties of the turbocharger are calculated from measurements on a thermohydraulic test bench described in [21] and following the procedure explained in [22]. On the other hand, measurements in a hot flow gas stand allowed to obtain the correlations for both internal heat transfer [23] and external heat transfer [24]. In addition, in order to adapt a mathematical model for turbocharger mechanical losses as described in [25], adiabatic measurements from gas stand have been used. Therefore, using these models, the calculation of heat transfer and mechanical losses for any operating condition of the turbocharger in the engine is possible.
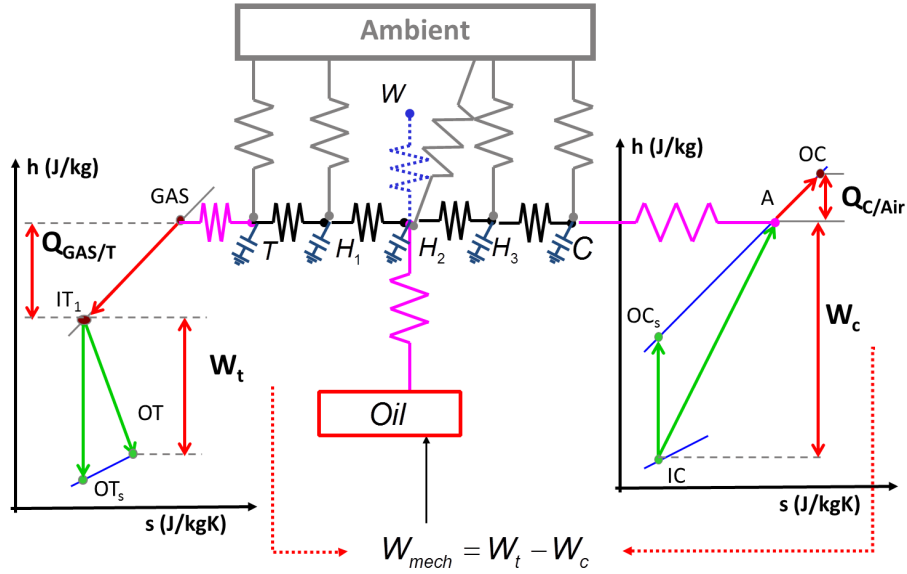

Figure 2: 1D lumped model

All the provided data make possible the correct computation of the model parameters in order to use it coupled with GT-Power, in a similar way to the work
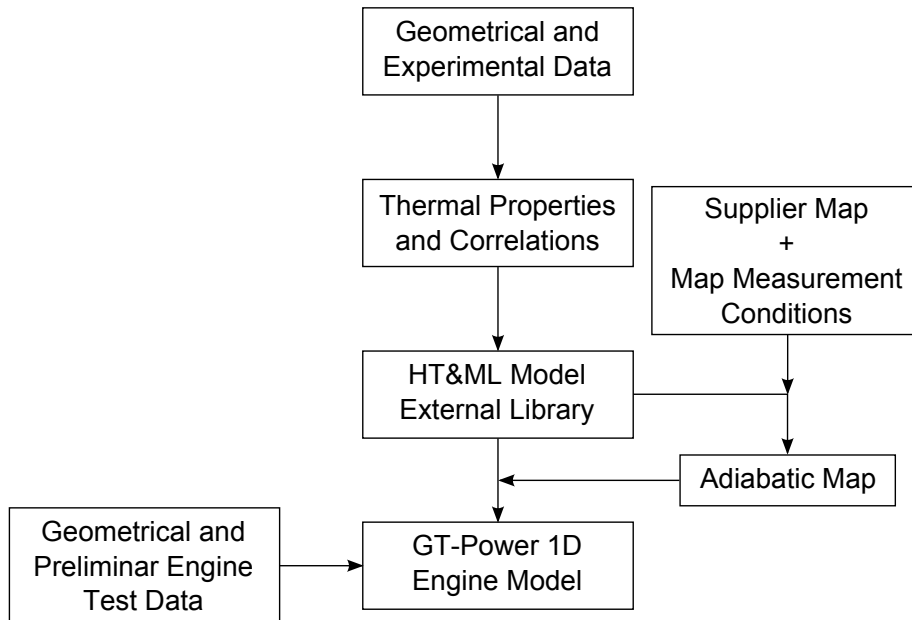
Figure 3: Modelling procedure

done in [26] in which only gas stand data have been analysed. The procedure is
outlined in Figure 3, which shows that HT&ML model is built on the basis of
thermal properties and heat transfer correlations for convection. Those corre-
lations have been obtained from test campaigns on both thermohydraulic test
bench and gas stand and from turbocharger simple geometrical data (detailed
geometry is not needed). The model for a given turbocharger is programmed in
an external library for further use. It is important to take into account that the
HT&ML model coupled with the engine model uses adiabatic compressor and
turbine performance maps. These maps can be obtained from direct adiabatic
measurements or from supplier (or hot) maps using the HT&ML in the inverse
form, i.e. removing the heat from the measured hot map [23]. For that inverse
use additional information about map measurement conditions (temperatures,
mass flows, etc.) is needed. Using the described arrangement, simulations in
GT-Power can be performed taking into account the turbocharger heat trans-
fer and mechanical losses model and using on engine test data for boundary

165

170

175

conditions definition.

3.2. Engine model

The engine model was built in GT-Power using, among others, the data and
tests mentioned in previous sections. A general scheme of the engine model in
GT-Power is shown in Figure 4. The HT&ML model has been introduced in
the engine model acting on the compressor, turbine and shaft variables in order
to take into account the heat transfer and mechanical losses phenomena in the
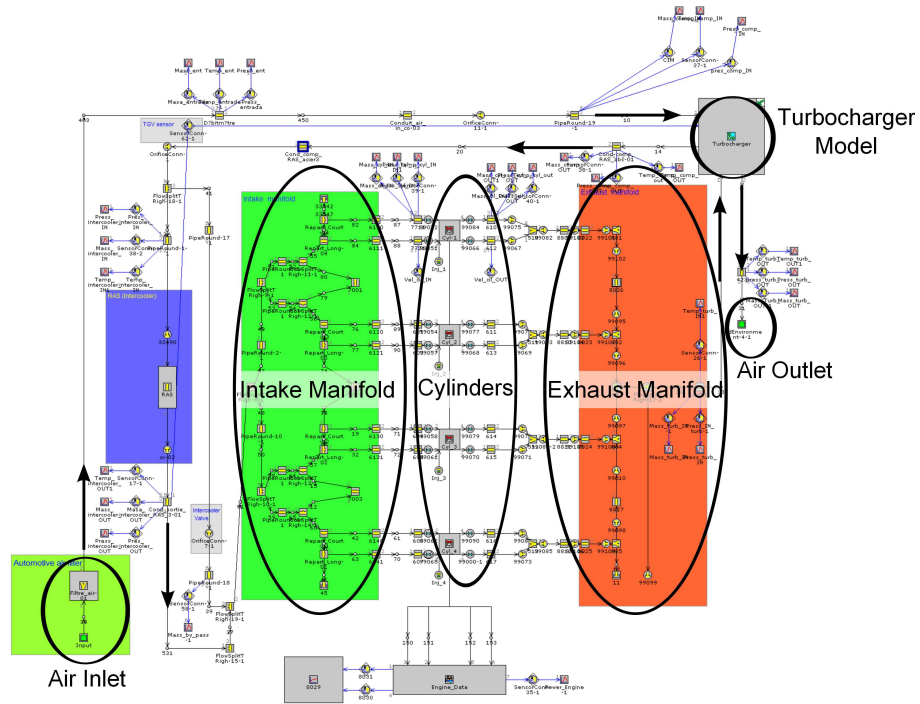turbocharger during the simulation.

Figure 4: Engine Model in GT-Power

In order to assure correct turbine inlet conditions the in-cylinder instanta-
neous variables values provided by the model have been analysed. As it had
been described in section 2.3, heat release laws obtained by an in-house combus-
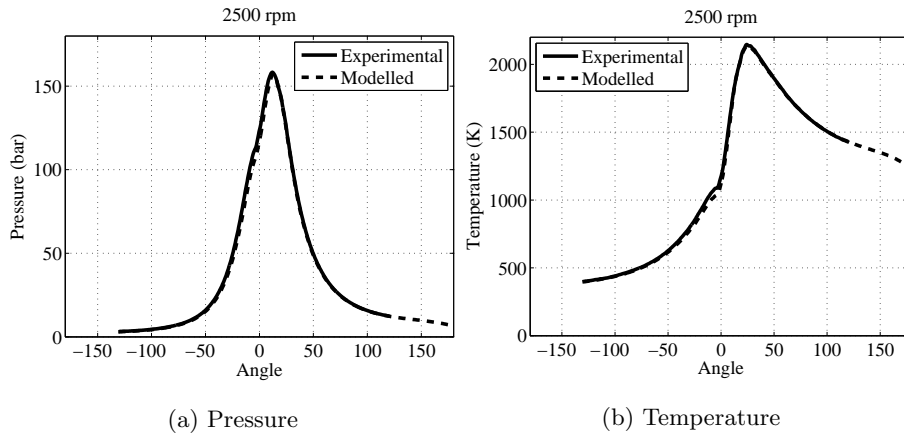tion diagnosis tool (CALMEC^{TM}) have been imposed in the cylinder, so GT-

(a) Pressure   (b) Temperature

Figure 5: In-cylinder pressure and temperature for T#1 at 2500 rpm and full load (2.0 litres engine)
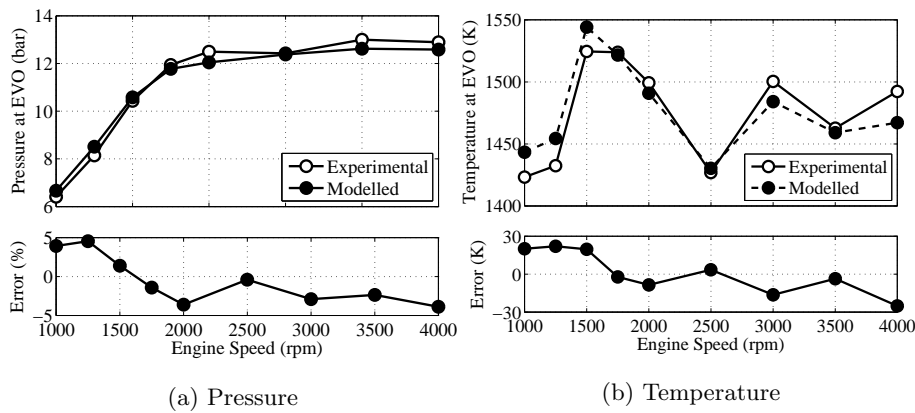

(a) Pressure   (b) Temperature

Figure 6: In-cylinder pressure and temperature at EVO for T#1 (2.0 litres engine)

Power inbuilt heat release models have not been used. Moreover, in-cylinder heat transfer coefficients have been adjusted in order to meet in-cylinder measured values. In Figure 5 instantaneous in-cylinder pressure and temperature are shown comparing the modelled values with instantaneous experimental values for a given engine speed. The differences are small, a fact that validates in-cylinder heat transfer coefficients adjustment. It can be observed, in Figure

15

6, that in-cylinder pressure at exhaust valve opening is also very similar for all the modelled engine speeds, being the errors within ±5%. The same holds for temperature, where errors are in the range of ±20 K, using the same set of in-cylinder heat transfer coefficients for all calculated engine speeds. Identical results from in-cylinder variables have been obtained using the HT&ML or not (for that reason only one curve for modelled values is shown in Figures 5 and 6), meaning that in-cylinder conditions are not affected by turbocharger HT&ML model in the modelled cases, what indicates that any difference in cylinder outlet variables (primary the turbine inlet temperature), cannot be caused by the use of HT&ML model.

3.3. Model results

The simulations performed on the GT-Power engine model were made in full load conditions using two different configurations:

- Original GT-Power turbocharger model, using turbine and compressor maps measured in a gas stand at hot conditions which includes turbocharger friction losses in the effective turbine efficiency (ETE). That fact means that ETE, shown in Equation 3, is used as provided by the turbocharger manufacturer. This is the standard practice.

$$\eta_{t,map} = ETE = \frac{\dot{m}_c \cdot c_{p,c} \cdot (T_{20} - T_{10})}{\dot{m}_t \cdot c_{p,t} \cdot (T_{30} - T_{4s})} = \frac{\dot{W}_c + \dot{Q}_{C/Air}}{\dot{W}_{ts}} \qquad (3)$$

- HT&ML model programmed in GT-Power, using turbine and compressor adiabatic maps. This is the new approach that is intended to be evaluated.

The results of T#1 will be represented versus the real engine speed. On the contrary, the results of the T#2 will be plotted versus an emulated engine speed. For this last turbocharger, engine speed was lowered during the tests to keep adequate volumetric flow due to the use of a 2.0 litres engine instead of 1.6 litres engine, as it had been explained in section 2.2. The results of both configurations have been compared with experimental data from the tests described in section 2.3.

3.3.1. Model prediction validation

Figure 7 and Figure 8 compare the results of the models with the experi-
mental data in torque and air mass flow. Good agreement has been achieved
using both configurations (with and without HT&ML model). As it can be ob-
served, from the point of view of these two parameters, related with the engine
behaviour, the differences between both configurations are insignificant.
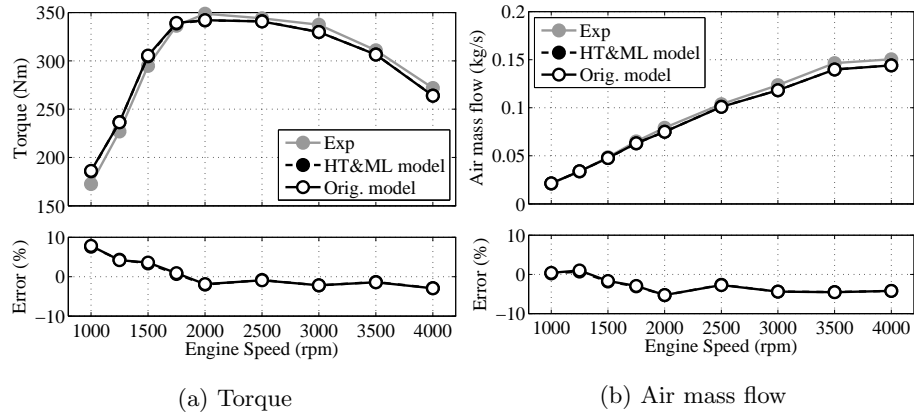

(a) Torque

(b) Air mass flow

Figure 7: Engine variables T#1. Actual 2.0 litres engine
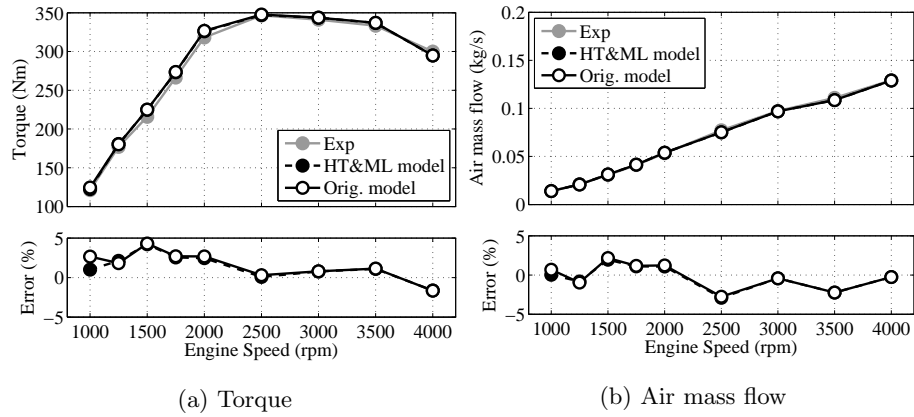

(a) Torque

(b) Air mass flow

Figure 8: Engine variables T#2. Emulated 1.6 litres engine

Figure 9 and Figure 10 show compressor parameters for both turbocharg-

17

ers. From the point of view of pressure ratio the HT&ML model offers similar results to those calculated without using it. Both models present a good agreement between modelled pressure ratio and experimental data due to the fact that a PID controller is used to impose experimental boost pressure. It must be reminded that original model uses the compressor map measured in hot conditions while in case of HT&ML model the compressor map used is the adiabatic one, i.e. it does not include the effect of the heat transfer that will have to
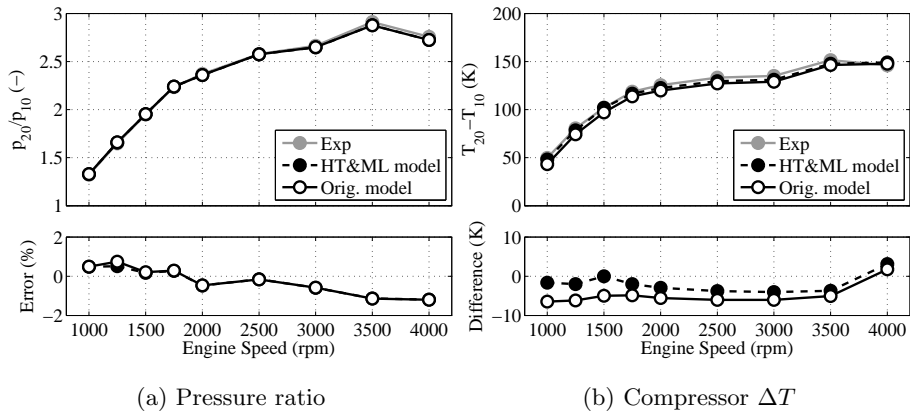

(a) Pressure ratio   (b) Compressor ΔT

Figure 9: T#1 Compressor pressure ratio and temperature increment

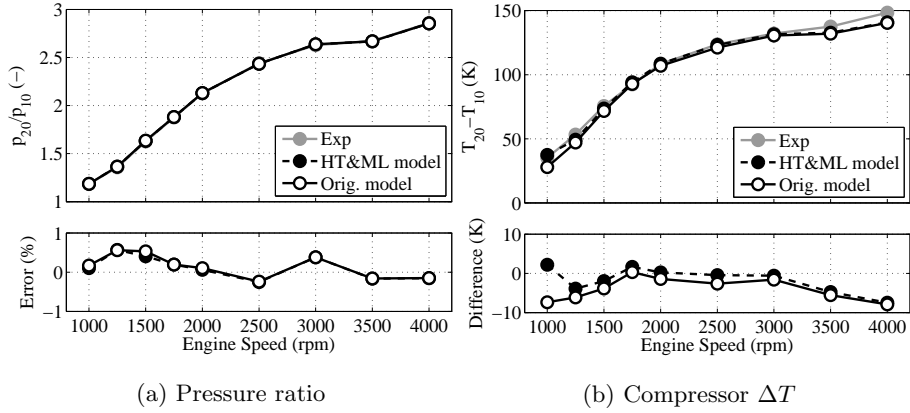(a) Pressure ratio   (b) Compressor ΔT

Figure 10: T#2 Compressor pressure ratio and temperature increment

be provided by the HT&ML model. Pressure ratio against mass flow maps are

18

identical with and without HT&ML model [26] and the effect of heat transfer is reflected in the compressor efficiency [27] i.e. in the air temperature incre-ment across the compressor. Compressor outlet temperature is related with the compression ratio (both cases have the same value) and the efficiency, so this parameter is affected by heat transfer and must be used properly. In the case of the original model the heat transfer effects are included in the map efficiency which is only valid when simulation conditions are similar to the conditions during map measurement. In the case of the new approach (using a HT&ML model), the employed efficiencies are adiabatic, so point '20a' in Figure 11 can be obtained. Furthermore, heat transfer in the compressor is computed using HT&ML model taking into account simulation conditions so adding that heat flow makes possible the calculation of the final COT (point '20' in Figure 11).

The definition of efficiencies in adiabatic and in hot (diabatic) maps are presented in Equations 4 and 5, where the temperature definitions are shown in Figure 11.

$$\eta_{c,adiab.} = \frac{T_{20s} - T_{10}}{T_{20a} - T_{10}} = \frac{\dot{W}_{cs}}{\dot{W}_c} \tag{4}$$

$$\eta_{c,diab.} = \frac{T_{20s} - T_{10}}{T_{20} - T_{10}} = \frac{\dot{W}_{cs}}{\dot{W}_c'} = \frac{\dot{W}_{cs}}{\dot{W}_c + \dot{Q}_{C/Air}} \tag{5}$$

The hot map includes the effect of the heat transfer and mechanical losses in the turbocharger for the map measurement conditions. For this reason, the prediction of a model using hot maps, in principle, will be accurate if the conditions of turbine inlet temperature and oil inlet temperature are similar between the modelled and the experimental ones when the maps were measured. Since T_{20} can be derived from the diabatic compressor efficiency ($\eta_{c,diab.}$) by using Equation 5.

The simulations of this paper for the original model use a hot map, where the map measurement temperatures were similar to those measured at full load engine conditions. If the map conditions were different, the measured diabatic
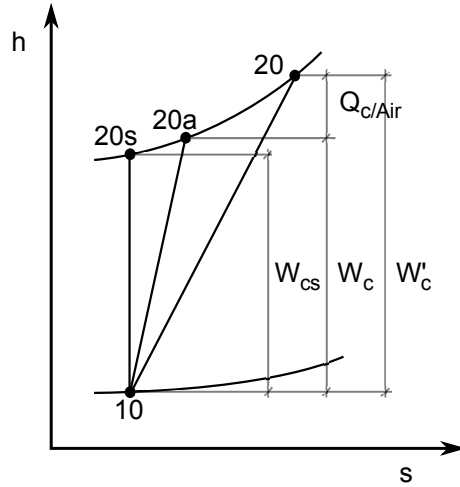
19

Figure 11: Enthalpy–entropy chart of the compression process

efficiency would be also different. Then compressor outlet temperature prediction would be worse than the results shown in Figures 9b and 10b.

On the contrary, HT&ML model uses adiabatic map, i.e. considering that the air is only heated due to the compression process and the internal irreversibilities. The heat transfer model estimates the heat to or from the compressor ($\dot{Q}_{C/Air}$) for each operating condition and this heat is added/removed at the compressor outlet as can be observed in Figures 2 and 11. So, the same T_{20} is obtained in both cases: using a hot map measured with identical temperature conditions than in engine measurements and using the evolution given by $\eta_{c,diab.}$ and using a two step evolution given by the efficiency $\eta_{c,adiab.}$ of an adiabatic map and the additional heat power ($\dot{Q}_{C/Air}$) of the HT&ML. For this reason, the differences observed between the results obtained using the HT&ML and those obtained with the original model are small. However, when the conditions of the map are not similar, HT&ML would still give the same result while the original model may underpredict or overpredict COT.

In spite of this, HT&ML model shows better results, specially at the low speed range (below 2000 rpm) as in Figure 9b and 10b. It is due to the fact that generally the heat transfer in the compressor is very small in comparison

to the compressor power except for very low turbocharger speed, as it has been studied in [28]. Despite of these small differences, up to 10 K improvement is observed using HT&ML model which is more relevant for the higher power water cooled turbocharger (T#1).

Figure 12 and Figure 13 compare modelled pressure ratio and temperature drop at the turbine versus experimental data for both turbochargers. Once again, significant differences have not been detected between both configurations from the point of view of pressure ratio. Only in the case of the lowest engine speed (1000 rpm) and T#2 (Figure 13), some improvements are obtained.
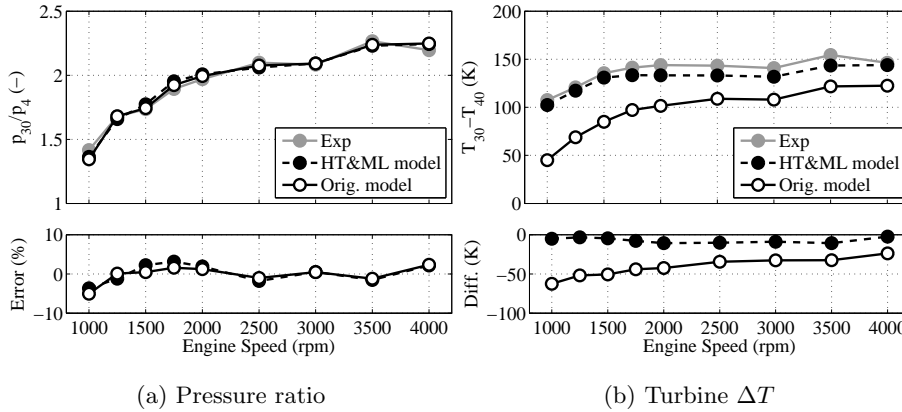

(a) Pressure ratio (b) Turbine ΔT

Figure 12: T#1 Turbine pressure ratio and temperature drop

The most significant differences between both models appear in temperatures. Supplier turbine map, used by GT-Power includes the effect of the heat transfer and the mechanical losses as has been shown in Equation 3. This allows the accurate prediction of the turbine power only if the turbine inlet conditions are equal to those used to measure the map. On the contrary, HT&ML model calculates the heat transfer and mechanical losses for every simulated engine conditions, for that reason it uses an adiabatic map where the efficiency, expressed in Equation 6, represents only the internal irreversibilities in the turbine flow. The heat ($\dot{Q}_{GAS/T}$) is extracted from the gas before it is expanded in the turbine stator (see Figure 2 and Figure 14). Additionally, the turbocharger
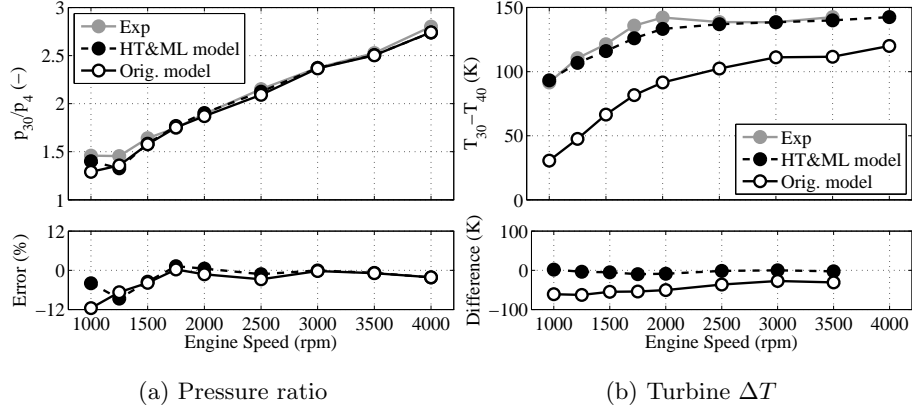
(a) Pressure ratio   (b) Turbine ΔT

Figure 13: T#2 Turbine pressure ratio and temperature drop

300   mechanical loses are removed directly in the shaft.

$$\eta_{t,adiab.} = \frac{T_{30a} - T_{4a}}{T_{30a} - T_{4as}} = \frac{\dot{W}_t}{\dot{W}_{tsa}} \tag{6}$$
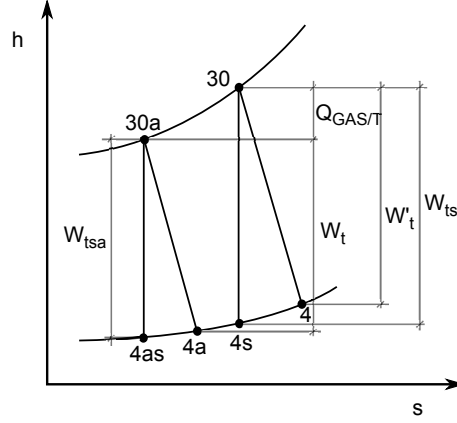

Figure 14: Enthalpy–entropy chart of the expansion process

In both simulation sets, the predicted turbine inlet temperature shows similar values due to the fact that this parameter is almost independent of the model used as it has been explained in section 3.2. The most important difference is observed in turbine outlet temperature. Figure 12b and Figure 13b

22

show that without HT&ML model turbine temperature differences arrive up to $-70K$ at low end torque conditions and original model never get differences below $-20K$. These errors contrast with the accurate results obtained with the HT&ML model where maximum errors are around $5K$. Using the hot map, the gas undergoes an enthalpy drop related with the isentropic turbine enthalpy drop and the ETE mapped efficiency. This process is represented in Figure 14 between points '30' and '4' where $W_t^{'} = W_c^{'} + W_{mech}$. Using the HT&ML model, the heat losses $(Q_{GAS/T})$ have been also considered , consequently, the enthalpy drop undergone by the gas is higher and much more realistic, following the points '30', '30a' and '4a' in Figure 14, where the evolution between '30a' and '4a' is given by the efficiency of an adiabatic map. As it can be observed the HT&ML model is able to predict correctly the temperature in the turbine outlet. This result is very important in order to model the different after-treatment elements placed in the exhaust line or any exhaust energy recovery device, like second stage turbochargers and bottoming ORC.

Figure 15 shows a comparison of turbocharger speed for both turbochargers. Good agreement has been obtained for both configurations due to the fact that boost pressure and mass flow through the compressor are controlled. Differences in this parameter can appear due to errors in the compressor map used or in the volumetric efficiency estimated by the engine model. The differences between both models are negligible, fact that will be recalled in the discussion of results section.

3.3.2. HT&ML model additional features

The developed model provides additional analysis capabilities which allows a deeper understanding of the different energetic transformations in the turbocharger. For example, Figure 16 compares the compressor efficiency for the full load test using different definitions. On one hand, adiabatic efficiency (Equation 4) can be provided by the HT&ML model and it compares mechanical compressor power versus isentropic compressor power. On the other hand, the diabatic efficiency can obtained from the temperature drops in the compressor
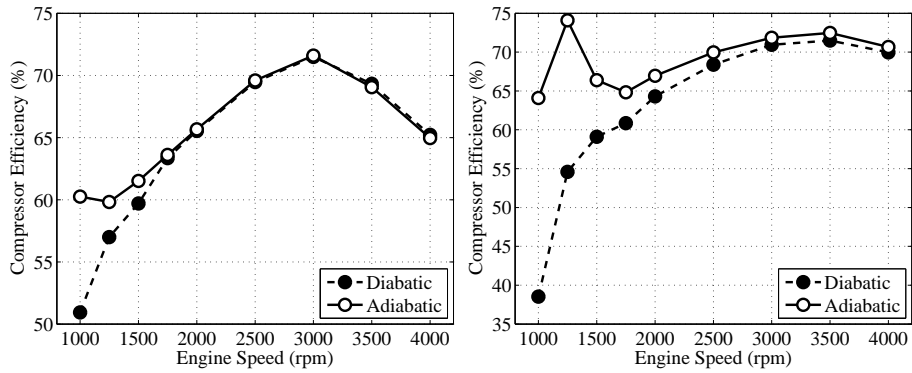
23
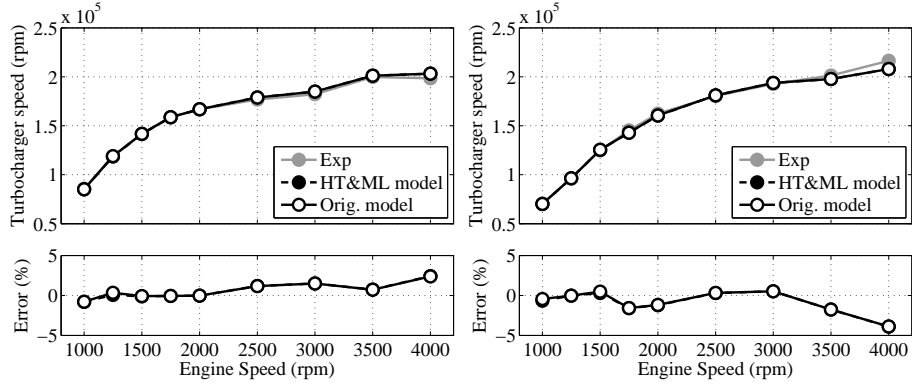
Figure 15: T#1 and T#2 turbocharger speed

and it includes the effect of the heat transfer. It must be taken into account that the powers are instantaneous variables obtained as a result of a non-linear calculation and the temperatures are weighted with instantaneous mass flow as shown in Equation 7.

$$\eta_{c,diab.}^{model} = \frac{\sum \dot{W}_{cs}^i}{\sum \dot{W}_c^i} = \frac{\sum \dot{m}_c^i \cdot \Delta T_s^i}{\sum \dot{m}_c^i \cdot \Delta T^i} \tag{7}$$

Figure 16: T#1 and T#2 compressor efficiency

Using T#1, which is water cooled, both compressor efficiencies are very sim-

24

ilar from 2000 rpm in advance due to the small heat transfer in the compressor compared with mechanical power, proving that water-cooling makes a thermal barrier from turbine to compressor as it was also pointed in [29]. At low engine speed, as the relative heat transfer effect increases, the compressor diabatic efficiency decreases. In the case of T#2, for all engine speeds the compressor receives heat power coming from the turbine. This phenomenon is much more important at low engine speed. In these conditions, the compressor outlet temperature increases due to heat transfer and, as a consequence, the diabatic efficiency decreases.

Similar analysis can be performed for the turbine. In this case four different definitions for the turbine efficiency can be used. The first efficiency definition is the most used in turbine maps provided by suppliers and it compares total compressor power with the turbine isentropic power. This definition, called ETE (Effective Turbine Efficiency), includes the effects of the heat transfer in turbine and compressor and the mechanical losses in the shaft, as it has been stated previously (Equation 3). It is important to note that ETE definition uses W_{ts} instead of W_{tsa}, since W_{tsa} is unknown without a HT model, as shown in Figure 14. The second definition for turbine efficiency compares mechanical power of the turbine versus isentropic power and is called adiabatic efficiency (Equation 6). If the mechanical efficiency is included in the definition, the result is given in Equation 8. Finally, the last definition can be obtained from the temperatures at turbine inlet and outlet. It is called diabatic efficiency which is shown in Equation 9 weighted with instantaneous mass flow. This definition is not commonly used since, in some cases, it can provide values higher than one or even lower than zero [26]. It includes the effect of heat transfer in the turbine that can be very important. When this effect is important T_4a can become lower than T_{4s} giving values higher than one. For that reason when heat losses are important compared to turbine power the diabatic efficiency does not represent the actual aerodynamic efficiency of the turbine.

$$\eta_{t,adiab.}^{model} \cdot \eta_{mech}^{model} = \frac{\dot{W}_t}{\dot{W}_{tsa}} \frac{\dot{W}_c}{\dot{W}_t} = \frac{\dot{W}_c}{\dot{W}_{tsa}} = \frac{\sum \dot{m}_t^i \cdot c_{p,c}^i \cdot (T_{20a} - T_{10})^i}{\sum \dot{m}_c^i \cdot c_{p,t}^i \cdot (T_{30a} - T_{4as})^i} \quad (8)$$

$$\eta_{t,diab.}^{model} = \frac{\sum \dot{m}_t^i \cdot (T_{30} - T_{4a})^i}{\sum \dot{m}_t^i \cdot (T_{30} - T_{4s})^i} = \frac{\dot{W}_t + \dot{Q}_{GAS/T}}{\dot{W}_{ts}} \quad (9)$$
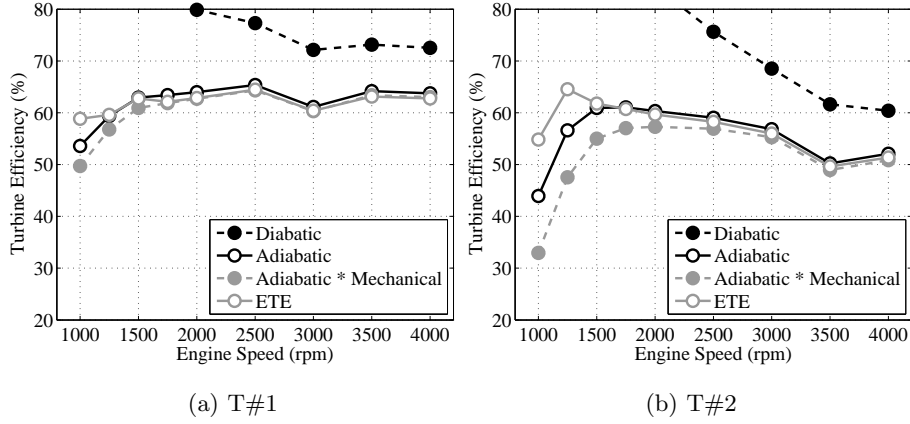

(a) T#1   (b) T#2

Figure 17: T#1 and T#2 turbine efficiency

Figure 17 compares the four turbine efficiencies for the full load engine tests, where obtained values for diabatic efficiency higher than 80% have been removed. It shows that diabatic efficiency is very high (in some cases higher than one), the reason is the lower turbine outlet temperature caused by the heat transfer in the turbine. This effect is more noticeable at lower speeds because turbine heat losses are higher, in relative terms, compared to turbine power. The difference between adiabatic (Equation 6) and adiabatic times mechanical (Equation 8) represents the turbocharger friction losses, and hence the adiabatic efficiency is always higher. In general, the effect of the friction losses in the turbocharger is more important at low engine speed (i.e. low turbocharger speeds). Comparing ETE (Equation 3) with the product of adiabatic and mechanical efficiencies (Equation 8), the differences are caused by the inclusion of the heat in the compressor ($\dot{Q}_{C/Air}$) and the different turbine isentropic power

used in both definitions ($\dot{W}_{tsa}$ or $\dot{W}_{ts}$). As can be observed the differences between these two definitions are more important when the turbocharger is not water-cooled (T#2), what increases the transfer of heat power from bearing housing to the compressor. In the case of T#1, due to water cooling, only at 1000 rpm appears a big difference between the three definitions.

Finally, an important parameter to analyse is turbocharger efficiency because of its influence on engine performance. If HT&ML is used, the turbocharger efficiency is calculated according to Equation 10, while for simulations without HT&ML, this efficiency is given by Equation 11. In the first case, an adiabatic map is used to compute turbocharger efficiency, whereas, in the second case, a hot map is used for the purpose. For both of these parameters, the calculations of the values from the models are obtained averaging the pulsating power.

$$\eta_{TG,adiab.}^{model} = \eta_{t,adiab.}^{model} \cdot \eta_{c,adiab.}^{model} \cdot \eta_{mech}^{model} = \frac{\dot{W}_t}{\dot{W}_{tsa}} \frac{\dot{W}_{cs}}{\dot{W}_c} \frac{\dot{W}_c}{\dot{W}_t} = \frac{\dot{W}_{cs}}{\dot{W}_{tsa}} \qquad (10)$$

$$\eta_{TG,map}^{model} = ETE \cdot \eta_{c,diab.}^{model} = \frac{\dot{W}_c + \dot{Q}_{C/Air}}{\dot{W}_{ts}} \frac{\dot{W}_{cs}}{\dot{W}_c + \dot{Q}_{C/Air}} = \frac{\dot{W}_{cs}}{\dot{W}_{ts}} \qquad (11)$$

It is worth noting that the simplification given in Equation 11 is possible only if compressor heat $\dot{Q}_{C/Air}$ is equal in ETE and compressor diabatic efficiency. This fact occurs only when turbine and compressor maps are measured at the same time without disassembling the turbocharger. With this assumption, the difference between both turbocharger efficiency definitions is just the turbine isentropic power ($\dot{W}_{tsa}$ or $\dot{W}_{ts}$). As it can be deduced from Figure 14, at high pressure ratios the relative difference between both isentropic powers will be small. Pressure ratio increases when engine speed (and also turbocharger speed increases), so at high speeds both turbine isentropic enthalpy drops will be similar. Figure 18a shows clearly this situation at high engine speeds and full load. That is when the difference between the values given by Equation 10 and Equation 11 will be small. Consequently, this effect of turbocharger heat transfer ($\dot{W}_{tsa}$ vs $\dot{W}_{ts}$) on turbocharger efficiency (defined in Equations 10 and 11) is low at high engine speeds.
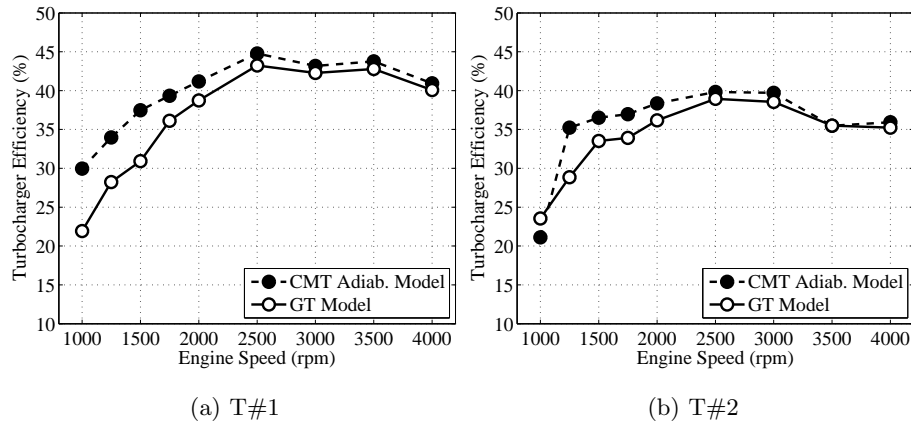
27

(a) T#1   (b) T#2

Figure 18: T#1 and T#2 turbocharger efficiency

When the turbocharger is working on the engine, heat and mechanical energy is transferred between the different elements. Using the information provided by the model, energy balances in the turbocharger can be computed from the point of view of heat power exchanged.

Figure 19 represents this heat balance for all full load working points. For T#2 (Figure 19b) the comparison is easier since, in this case, only the turbine losses heat. This behaviour occurs when the compressor just absorb the heat coming from the turbine. For the oil it is a predictable behaviour as it works as a heat sink in the absence of water cooling. For the compressor the sign of heat flow depends on the operating conditions.

At high pressure ratios, the compressor can lose heat that will be absorbed by the oil, ambient or the water (as shown in Figure 19a for T#1 when the engine is running at 3500 rpm and 4000 rpm). Figure 19b also shows how the heat is distributed in T#2. More than 50% of the heat losses in the turbine go to the ambient and this percentage increases at higher engine speeds. This result extracted from the HT&ML model is in concordance with different studies of other authors such as [30]. The compressor receives similar heat power for all engine speeds in absolute value only slightly higher at low engine speeds. Nevertheless, this heat in relative terms and at high engine speed is negligible
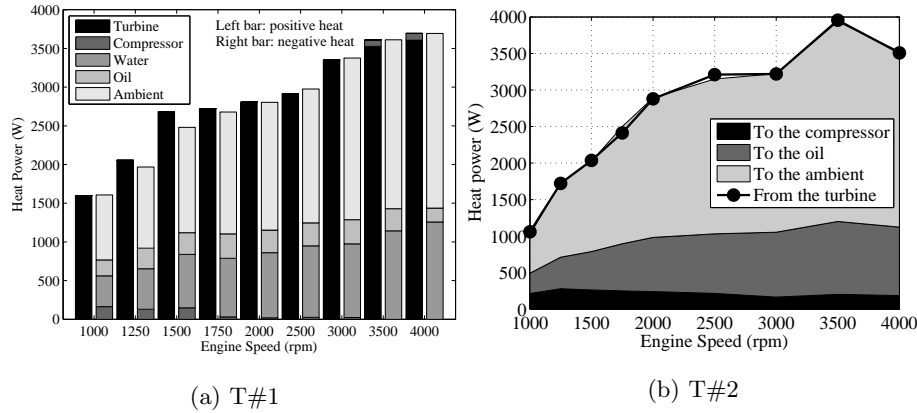
(a) T#1

(b) T#2

Figure 19: T#1 and T#2 heat power balance

in comparison to compressor power. In Figure 19a for T#1, each engine test is represented by two different bars. The left bar is the sum of all heats flowing to the metal parts of the turbocharger and right bar is the sum of all heats flowing from the metal parts. In this case, turbine casing always losses heat power that is always received it by the ambient, the water and the oil. However, the heat flow in the compressor can change its direction (from/to central housing) depending on the operating conditions, as has been stated previously. In this case the ambient is again the node that receives a higher rate of heat and the oil receive low heat quantity due to the water-cooling. However, the compressor air at the engine speeds of 3500 rpm and 4000 rpm losses heat (positive sign) since it works with high pressure ratios, while at lower engine speeds (i.e. lower pressure ratios) the compressor air receives heat (negative sign).

Using the HT&ML a turbocharger mechanical power balance can be also performed. Figure 20 represents this balance where a logarithmic y-axis has been used to remark the different orders of magnitude among turbine and compressor mechanical powers and turbocharger friction losses power. As can be observed in Figure 20, despite the fact that the mechanical losses are higher at high engine speed tests, the effect of these losses is much more important at low engine speed points because compressor and turbine power decrease faster than mechanical

29

losses at low engine speeds.
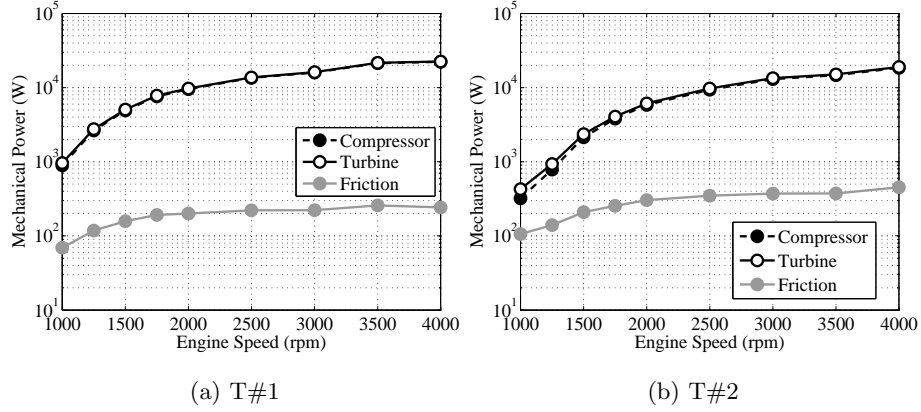

(a) T#1

(b) T#2

Figure 20: T#1 and T#2 mechanical power balance

4. Discussion of results

The comparison between the results of both kind of simulations and the experimental data shows that COT and TOT prediction is the main substan-
450 tial improvement using a heat transfer and mechanical losses model for the turbocharger. This improvement is crucial in inter-cooling [31], combustion process [32] where there is no intercooler, aftertreatment [33], exhaust energy recovery [34], exhaust heat transfer modelling [35] and two stage turbocharging [36] modelling. Even the simulation of full load conditions can be improved us-
455 ing HT&ML model. However, the improvements of the model result only in the prediction of COT and TOT and do not affect the engine performance variables if the turbocharger map, used in the original configuration, is chosen properly. This map must have been measured in similar conditions to those desired to be modelled, so turbocharger manufacturer maps that hold this condition are suit-
460 able to be used in order to predict well all the variables associated to the engine excepting TOT. Cold maps can also be used but always coupled with a HT&ML model. In that case the prediction of all variables, including TOT is precise. The turbo speed is not affected by the different models as it has been shown in this

work and it has been demonstrated by the development shown in Equations 12, 13 and 14 showing turbocharger speed increment, where K primarily depends on turbocharger shaft inertia and time step. Previously in Equation 12 ETE definition is derived; where the compressor mechanical power has been replaced by the product of mechanical efficiency and turbine mechanical power. Since the only difference between $\dot{W}_{ts}$ and $\dot{W}_{tsa}$ is the turbine inlet temperature, it is possible to introduce turbine adiabatic efficiency in the equation as has been done in Equation 12.

$$ETE = \frac{\eta_{mech} \cdot \dot{W}_t + \dot{Q}_{C/Air}}{\dot{W}_{ts}} = \left(\eta_{mech} \cdot \eta_{t,adiab.} + \frac{\dot{Q}_{C/Air}}{\dot{W}_{tsa}} \right) \frac{T_{30a}}{T_{30}} \qquad (12)$$

In Equation 13, the turbo speed increment expression has been derived using the HT&ML model approach. The resulting equation is function of compressor and turbine adiabatic efficiencies, turbocharger friction losses efficiency and isentropic power of compressor and turbine.

$$
\begin{aligned}
\Delta N & = K \left(\dot{W}_t - \dot{W}_{mech} - \dot{W}_c \right) = \\
& = K \left(\eta_{mech} \cdot \dot{W}_t - \dot{W}_c \right) = \\
& = K \left(\eta_{mech} \cdot \eta_{t,adiab.} \cdot \dot{W}_{tsa} - \frac{\dot{W}_{cs}}{\eta_{c,adiab.}} \right) \qquad (13)
\end{aligned}
$$

In Equation 14, the turbo speed increment expression has been derived using the original model approach, i.e using map efficiencies definitions (ETE and $\eta_{c,diab.}$). Introducing Equations 5 and 12 and it gives the same expression as in Equation 13.

$$
\begin{aligned}
\Delta N & = K \left(\dot{W}_t' - \dot{W}_c' \right) = \\
& = K \left(ETE \cdot \dot{W}_{ts} - \frac{\dot{W}_{cs}}{\eta_{c,diab.}} \right) = \\
& = K \left(ETE \cdot \frac{T_{30}}{T_{30a}} \cdot \dot{W}_{tsa} - \frac{\dot{W}_{cs}}{\eta_{c,diab.}} \right) =
\end{aligned}
$$

31

$$= K \left(\eta_{mech} \cdot \eta_{t,adiab.} \cdot \dot{W}_{tsa} + \dot{Q}_{C/Air} - \frac{\dot{W}_{cs}}{\eta_{c,diab.}} \right) =$$

$$= K \left(\eta_{mech} \cdot \eta_{t,adiab.} \cdot \dot{W}_{tsa} + \dot{Q}_{C/Air} - \left(\dot{W}_c + \dot{Q}_{C/Air} \right) \right) =$$

$$= K \left(\eta_{mech} \cdot \eta_{t,adiab.} \cdot \dot{W}_{tsa} - \frac{\dot{W}_{cs}}{\eta_{c,adiab.}} \right) \qquad (14)$$

So, it can be concluded that the usage of ETE definition for turbine efficiency without HT&ML is suitable if errors in turbocharger speed prediction are to be minimised in steady operating conditions and compressor and turbine maps were measured at same time to cancel $\dot{Q}_{C/Air}$ terms. As a drawback, the prediction of turbine outlet temperature is not satisfactory. Concluding, if a HT&ML model with an adiabatic map is used every variable prediction is satisfactory, while special care must be taken with turbine efficiency definition if simulations are performed without using a HT&ML.

5. Conclusions

In this paper full load tests for two different turbochargers have been simulated using a commercial 1D software and the results have been compared with the experimental data from an engine test bench. The main findings of this comparison lay in the fact that manufacturer maps in hot conditions are adequate in predicting all variables at engine full loads excepting COT and TOT. This fact shows the actual importance of using a heat transfer model for the turbocharger.

Compressor and turbine outlet temperatures are always well predicted using a heat transfer model without disturbing the prediction of the rest of engine parameters.

Contrary to the general view that heat transfer phenomena occurring in turbochargers are only important at partial loads and transient engine evolutions, in this work, it is shown that full load operating points are also affected by these phenomena. The compressor and turbine outlet temperatures are important variables to be predicted at these operating points. The importance is in

32

intercooler design (or combustion process), aftertreatment, exhaust energy recovery and two stage turbocharging modelling and design because accurately predicted boundary conditions can be used in each case.

Besides, the paper shows that turbo speed prediction is not affected by heat transfer when hot turbocharger maps in which compressor and turbine have been measured at the same time are used. The reason is the cancellation of compressor heat terms in this kind of maps. Only prediction of compressor and turbine outlet temperatures is improved by the heat transfer model, if they are compared to the model based on hot maps.

Finally, it has been shown that the information provided by the model can be used to perform turbocharger energy balances that shows the more important energy losses in the turbocharger as a function of engine speed.

Acknowledgements

References

[1] N. Baines, Intake Boosting, Encyclopedia of Automotive Engineering, John Wiley & Sons, Ltd., 2014. `doi:/10.1002/9781118354179.auto126`.

[2] L. Cornolti, A. Onorati, T. Cerri, G. Montenegro, F. Piscaglia, 1D simulation of a turbocharged Diesel engine with comparison of short and long EGR route solutions, Applied Energy 111 (2013) 1 – 15. `doi:/10.1016/j.apenergy.2013.04.016`.

[3] S. Marelli, C. Carraro, G. Marmorato, G. Zamboni, M. Capobianco, Experimental analysis on the performance of a turbocharger compressor in

₅₃₀   the unstable operating region and close to the surge limit, Experimental Thermal and Fluid Science 53 (2014) 154 – 160. `doi:/10.1016/j.expthermflusci.2013.11.025`.

[4] B. Sirakov, M. Casey, Evaluation of heat transfer effects on turbocharger performance, ASME Journal of Turbomachinery 135 (2) (2012) 021011. `doi:/10.1115/1.4006608`.

[5] A. Romagnoli, R. Martinez-Botas, Heat transfer analysis in a turbocharger turbine: An experimental and computational evaluation, Applied Thermal Engineering 38 (2012) 58 – 77. `doi:/10.1016/j.applthermaleng.2011.12.022`.

[6] M. V. Casey, T. M. Fesich, The efficiency of turbocharger compressors with diabatic flows, Journal of Engineering for Gas Turbines and Power 132 (7) (2012) 072302. `doi:/10.1115/1.4000300`.

[7] H. Aghaali, H.-E. Ångström, J. R. Serrano, Evaluation of different heat transfer conditions on an automotive turbocharger, International Journal of Engine Research 16 (2) (2015) 137–151. `doi:/10.1177/1468087414524755`.

[8] K. Chapman, R. Nguru, J. Shultz, Simplified Methodology to Correct Turbocharger Field Measurements for Heat Transfer and Other Effects: Topical Report, January 2000 - June 2002, Report: Gas Research Institute, Kansas State University, 2002.

[9] H. Aghaali, H.-E. Ångström, Turbocharged SI-Engine Simulation with Cold and Hot-Measured Turbocharger Performance Maps, in: Proceedings of ASME Turbo Expo, Vol. 5, ASME, 2012, pp. 671–679. `doi:10.1115/GT2012-68758`.

[10] P. Chesse, D. Chalet, X. Tauzia, Impact of the heat transfer on the performance calculations of automotive turbocharger compressor, Oil & Gas

Science and Technology – Rev. IFP Energies nouvelles 66 (5) (2011) 791 –
800. `doi:10.2516/ogst/2011129`.

[11] R. D. Burke, C. R. M. Vagg, D. Chalet, P. Chesse, Heat transfer in
turbocharger turbines under steady, pulsating and transient conditions,
International Journal of Heat and Fluid Flow 52 (0) (2015) 185 – 197.
`doi:/10.1016/j.ijheatfluidflow.2015.01.004`.

[12] A. Romagnoli, R. Martinez-Botas, Heat transfer in an automotive tur-
bocharger under constant load points: an experimental and computational
investigation, The 4th International Symposium on Fluid Machinery and
Fluid Engineering November 24-27, 2008, Beijing, China.

[13] R. D. Burke, C. D. Copeland, T. Duda, Investigation into the assumptions
for lumped capacitance modelling of turbocharger heat transfer, in: 6th
International conference on simulation and testing 2014-05-15 - 2014-05-
16, Berlin, 2014.

[14] H. Aghaali, H.-E. Ångström, Temperature estimation of turbocharger
working fluids and walls under different engine loads and heat trans-
fer conditions, SAE Technical Paper 2013-24-0123. `doi:/710.4271/
2013-24-0123`.

[15] Evaluation of measurement data – Guide to the expression of uncertainty
in measurement, JCGM.

[16] P. Olmeda, A. Tiseira, V. Dolz, L. García-Cuevas, Uncertainties in power
computations in a turbocharger test bench, Measurement 59 (0) (2015) 363
– 371. `doi:http://dx.doi.org/10.1016/j.measurement.2014.09.055`.

[17] F. Payri, A. J. Torregrosa, A. Broatch, J. Brunel, Pressure loss char-
acterisation of perforated ducts, SAE Technical Paper 980282. `doi:
/10.4271/980282`.

[18] F. Payri, P. Olmeda, J. Martín, A. García, A complete 0D thermodynamic predictive model for direct injection diesel engines, Applied Energy 88 (12) (2011) 4632 – 4641. `doi:/10.1016/j.apenergy.2011.06.005`.

[19] J. Benajes, P. Olmeda, J. Martín, R. Carreño, A new methodology for uncertainties characterization in combustion diagnosis and thermodynamic modelling, Applied Thermal Engineering 71 (1) (2014) 389 – 399. `doi:/10.1016/j.applthermaleng.2014.07.010`.

[20] P. Olmeda, V. Dolz, F. Arnau, M. Reyes-Belmonte, Determination of heat flows inside turbochargers by means of a one dimensional lumped model, Mathematical and Computer Modelling 57 (7–8) (2013) 1847 – 1852. `doi:/10.1016/j.mcm.2011.11.078`.

[21] A. J. Torregrosa, A. Broatch, P. Olmeda, J. Martín, A contribution to film coefficient estimation in piston cooling galleries, Experimental Thermal and Fluid Science 34 (2) (2010) 142–151.

[22] J. R. Serrano, P. Olmeda, A. Páez, F. Vidal, An experimental procedure to determine heat transfer properties of turbochargers, Measurement Science and Technology 21 (2010) 035109. `doi:/10.1088/0957-0233/21/3/035109`.

[23] M. Reyes-Belmonte, Contribution to the experimental characterization and 1-D modelling of turbochargers for IC engines, Ph.D. thesis, Universitat Politècnica de València, Valencia (2013).

[24] F. Payri, P. Olmeda, F. Arnau, A. Dombrovsky, L. Smith, External heat losses in small turbochargers: Model and experiments, Energy 71 (2014) 534 – 546. `doi:/10.1016/j.energy.2014.04.096`.

[25] J. R. Serrano, P. Olmeda, A. Tiseira, L. García-Cuevas, A. Lefebvre, Theoretical and experimental study of mechanical losses in automotive turbochargers, Energy 55 (2013) 888 – 898. `doi:10.1016/j.energy.2013.04.042`.

[26] J. R. Serrano, P. Olmeda, F. Arnau, A. Dombrovsky, L. Smith, Analysis and methodology to characterize heat transfer phenomena in automotive turbochargers, J. Eng. Gas Turbines Power 137 (7) (2014) 021901 (11 pages) Paper No: GTP–14–1352. `doi:/10.1115/1.4028261`.

[27] M. Cormerais, J. F. Hetet, P. Chesse, A. Malboom, Heat transfers characterization in a variable geometry turbocharger: experiments and correlations, Proceedings of Spring Technical Conference of the ASME Internal Combustion Engine Division (2006) 53 – 64.

[28] M. Cormerais, P. Chesse, J. F. Hetet, Turbocharger heat transfer modeling under steady and transient conditions, International Journal of Thermodynamics 12 (4) (2010) 193 – 202.

[29] D. Bohn, N. Moritz, M. Wolff, Conjugate Flow and Heat Transfer Investigation of a Turbo Charger: Part II — Experimental Results, in: Proceedings of ASME Turbo Expo, Vol. 3, ASME, 2003, pp. 723–729. `doi:10.1115/GT2003-38449`.

[30] N. Baines, K. D. Wygant, A. Dris, The analysis of heat transfer in automotive turbochargers, Journal of Engineering for Gas Turbines and Power 132 (4) (2010) 042301. `doi:/10.1115/1.3204586`.

[31] C. Cuevas, D. Makaire, P. Ngendakumana, Thermo-hydraulic characterization of an automotive intercooler for a low pressure EGR application, Applied Thermal Engineering 31 (14–15) (2011) 2474 – 2484. `doi:/10.1016/j.applthermaleng.2011.04.013`.

[32] M. Canakci, Combustion characteristics of a DI–HCCI gasoline engine running at different boost pressures, Fuel 96 (2012) 546 – 555. `doi:/10.1016/j.fuel.2012.01.042`.

[33] J. M. Luján, V. Bermúdez, P. Piqueras, Óscar García-Afonso, Experimental assessment of pre-turbo aftertreatment configurations in a single stage turbocharged diesel engine. part 1: Steady-state operation, Energy 80 (0)

37

(2015) 599 – 613. `doi:http://dx.doi.org/10.1016/j.energy.2014.05.048`.

[34] V. Macián, J. R. Serrano, V. Dolz, J. Sánchez, Methodology to design a bottoming Rankine cycle, as a waste energy recovering system in vehicles. Study in a HDD engine, Applied Energy 104 (2013) 758 – 771. `doi:/10.1016/j.apenergy.2012.11.075`.

[35] J. M. Luján, H. Climent, P. Olmeda, V. D. Jiménez, Heat transfer modeling in exhaust systems of high-performance two-stroke engines, Applied Thermal Engineering 69 (1–2) (2014) 96 – 104. `doi:/10.1016/j.applthermaleng.2014.04.045`.

[36] J. Galindo, J. R. Serrano, H. Climent, O. Varnier, Impact of two-stage turbocharging architectures on pumping losses of automotive engines based on an analytical model, Energy Conversion and Management 51 (10) (2010) 1958 – 1969. `doi:/10.1016/j.enconman.2010.02.028`.